ChemComm

COMMUNICATION

View Article Online
View Journal | View Issue

Cite this: *Chem. Commun.*, 2019, 55, 4941

Received 13th January 2019,
Accepted 28th March 2019

DOI: 10.1039/c9cc00305c

rsc.li/chemcomm

A highly stable nanofibrous Eu-MOF membrane as a convenient fluorescent test paper for rapid and cyclic detection of nitrobenzene†

Ting-Ting Li,[ab] Lin Liu,*[a] Ming-Liang Gao[a] and Zheng-Bo Han *[a]

A stable fluorescent nanofibrous membrane was fabricated by *in situ* growing Eu-MOF crystals on electrospun polyacrylonitrile nanofibers modified with γ-aminobutyric acid. This nanofibrous membrane can be used as a convenient fluorescent test paper for rapid and cyclic detection of nitrobenzene.

Nitrobenzene (NB) is the basic and simplest constituent of explosives among various nitroaromatics. Moreover, NB is a highly toxic pollutant that can cause serious health and environmental problems. Therefore, the sensitive detection of NB has become a critical issue. Although various technologies such as gas chromatography coupled with mass spectrometry (GC-MS),[1] surface enhanced Raman spectroscopy (SERS),[2] cyclic voltametry[3] and ion mobility spectrometry (IMS)[4] have been developed for the detection of explosives, these methods are limited,[5] because GC-MS equipment is large-scale, SERS needs complex sample pretreatment and IMS instruments are expensive. Considering that NB can act as an excellent electron acceptor owing to its withdrawing nitro-group,[6] fluorescence quenching based on chemical sensing has been recognized as the sensitive and convenient method for the rapid detection of NB.[7] In view of this, exploring effective and reversible luminescence materials is very necessary.

Metal–organic frameworks (MOFs), a fascinating class of solid crystalline materials, have been considered as promising candidates for gas adsorption and separation due to their intrinsic porous characteristics and extraordinarily large surface area.[8] In recent years, great progress has been made in the use of MOFs as luminescence sensors for various species.[9] Due to their unique properties of short response times, characteristic sharp emission in the visible region and relatively long luminescence lifetimes,[10] lanthanide MOFs, especially Eu-MOFs, have been considered to be effective luminescent probes for sensing NB. However, most of the research[11] focused on powder crystalline materials. From the standpoint of separation and recovery of fluorescence sensors from detection systems, film sensors are more predominant compared with powdered materials because no separation process is needed for the films.

Electrospinning is a convenient and effective route to fabricate nanofibrous membranes (NFMs) with high porosity, large specific surface area, tunable structure and ease of surface modification.[12] Compared to thin films, electrospun NFMs have greater surface area approximately 1–2 orders of magnitude.[13] Recently, more attention has been paid to electrospinning because this versatile technique is able to convert MOF particles into self-supported and flexible MOF NFMs.[14] The preparation of electrospun MOF NFMs and their applications, such as air filtration,[15] gas capture,[16] and heavy/radioactive metal adsorption,[17] and sensing/detection,[18] have been reported. However, most of the MOF NFMs were fabricated *via* co-electrospinning of MOF crystals and polymers. In terms of luminescence sensors, the active sites of composite NFMs may be significantly reduced because MOF particles were encapsulated by polymers.[19] Hatton *et al.* grew MOF crystals directly on an electrospun polyacrylonitrile NFM using microwave irradiation technology,[20] but owing to the weak interaction of the MOF particles and polymer matrix, the MOF crystals were unstable and easily fell off the membrane.

In this study, we designed and fabricated a stable fluorescent NFM by *in situ* growing Eu-MOF crystals on electrospun polyacrylonitrile (PAN) nanofibers modified with γ-aminobutyric acid (GABA) (Scheme 1). The PAN NFM was employed as a matrix due to its robust mechanical strength, excellent water insolubility, good hydrophilicity and high chemical stability. In addition, the abundant active nitrile groups of PAN can be used for further derivatization. GABA performed well as a grafting agent, because not only can it introduce a great number of coordination sites (carboxyl groups) into the nanofibrous matrix for anchoring Eu-MOF particles, but its relatively long carbon chains can reduce

[a] College of Chemistry, Liaoning University, Shenyang 110036, P. R. China. E-mail: linliu@lnu.edu.cn, ceshzb@lnu.edu.cn
[b] College of Material Science and Engineering, North China University of Science and Technology, Tangshan, 063009, P. R. China

† Electronic supplementary information (ESI) available. See DOI: 10.1039/c9cc00305c

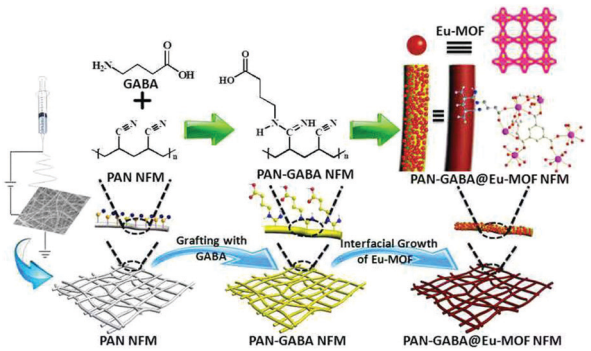

Scheme 1 Fabrication process of a PAN–GABA@Eu-MOF NFM.

the steric hindrance of both the grafting reaction and crystal growing process. GABA was grafted onto the surface of the PAN NFM first, and then Eu-MOF crystals were *in situ* grown on the PAN–GABA NFM. Benefiting from the integrated merits of the electrospun PAN NFM, GABA and Eu-MOF crystals, the as-prepared PAN–GABA@Eu-MOF NFM can be used as a convenient fluorescent test paper for rapid and cyclic detection of NB. More importantly, the fluorescent test paper exhibited high reversibility with stable quenching efficiency and a fast "off–on" fluorescence switching process.

The representative SEM image of PAN nanofibers is shown in Fig. 1a. These random nanofibers exhibited a smooth and uniform surface and had an average diameter of 152 ± 31 nm. After being grafted with GABA, a compact structure among fibers was formed along with the increase of the average fiber diameter to 258 ± 36 nm (Fig. 1b). This may be attributable to the graft polymerization of GABA and the impregnation of the solution into the fibers during the modification process. In order to ensure the compatibility and size suitability of the MOF crystals on the polymer nanofibers, the Eu-MOF particle size was tuned on the nanoscale by employing sodium acetate as the capping reagent (Fig. 1c). Fig. 1d displays an image of the PAN–GABA@Eu-MOF NFM. It was clear that the fibers exhibited a rough tree-bark-like surface, indicating the effective growth of Eu-MOF crystals on PAN–GABA nanofibers. As illustrated in the insets of Fig. 1, the optical photographs of PAN, PAN–GABA and PAN–GABA@Eu-MOF NFMs were white, yellow and dark yellow in natural light, respectively. The PAN–GABA@Eu-MOF NFMs emitted red color under a 265 nm UV lamp, as shown in Fig. S1 (ESI†). Eu-MOF crystals on the nanofibers increased with the increase of crystal growth time and the red color of the NFMs gradually became darker at the same time. When the growth time exceeded 12 h, there was a serious adhesion between the nanofibers (Fig. S1d, ESI†). In terms of the porosity and fluorescence of the PAN–GABA@Eu-MOF NFM, 12 h was used to conduct the following experiments.

The composition and structure of the as-prepared PAN–GABA@Eu-MOF NFM were characterized by EDS, FT-IR and PXRD. As shown in Fig. S2 and S3 (ESI†), C, N, O and Eu elements were detected as expected, and Eu element was distributed evenly on the surface of the NFM. Fig. 2a and Fig. S4 (ESI†) show the FT-IR spectra of the PAN, PAN–GABA, PAN–GABA@Eu-MOF NFMs and Eu-MOF crystals. The PAN NFM exhibited characteristic absorption peaks at 2243 cm^{-1}, corresponding to the stretching vibration of C≡N. After modification with GABA, the intensity of the peak associated with the nitrile group at 2243 cm^{-1} decreased obviously.

Meanwhile, new peaks at 1632, 1662 and 3200–3358 cm^{-1} appeared, which can be assigned to the stretching vibration of N–C=N, C=O and O–H, respectively.[21] All the changes indicated that GABA was successfully grafted onto the PAN NFM, and thus can provide a great number of carboxyl groups for growing Eu-MOF crystals. The FT-IR spectrum of the PAN–GABA@Eu-MOF NFM had nearly all the key features of those of the Eu-MOF crystals and PAN–GABA NFM. The peak at 1612 cm^{-1} was attributed to the skeletal vibration of the aromatic ring, and peaks at 700–800 cm^{-1} were related to the out-of-plane C–H bending vibrations of the substituted benzene compounds. These results provided preliminary evidence that Eu-MOF crystals were successfully grown on the surface of the PAN–GABA NFM. Fig. 2b shows that the experimental PXRD pattern of the Eu-MOF powder was consistent with the simulated one,[22] while two broad peaks appeared in the pattern of PAN–GABA in an amorphous form. The PXRD pattern of the PAN–GABA@Eu-MOF NFM, as expected, contained all the

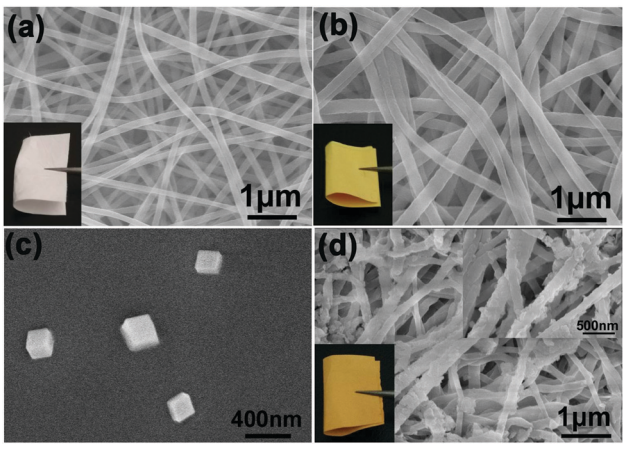

Fig. 1 SEM images of (a) PAN nanofibers, (b) PAN–GABA nanofibers, (c) Eu-MOF particles and (d) PAN–GABA@Eu-MOF nanofibers. The insets show the corresponding optical photographs of the samples and a high magnification SEM image of PAN–GABA@Eu-MOF nanofibers.

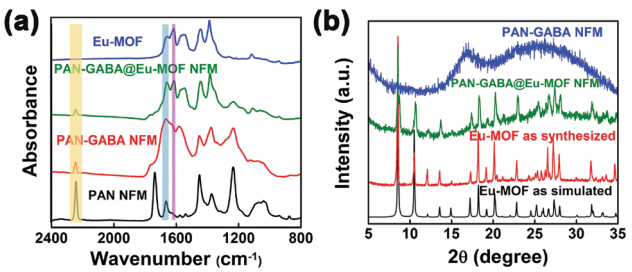

Fig. 2 (a) FT-IR spectra of PAN, PAN–GABA, and PAN–GABA@Eu-MOF NFMs and Eu-MOF crystals. (b) PXRD patterns of the Eu-MOF crystals, PAN–GABA NFM and PAN–GABA@Eu-MOF NFM.

peaks of the Eu-MOF crystals and PAN–GABA, further confirming the effective growth of Eu-MOF crystals on the PAN–GABA NFM.

The wettability of the PAN–GABA@Eu-MOF NFM was investigated by measuring the contact angle of methanol on the membrane. As can be seen from Fig. S5 (ESI†), the wettability of the PAN NFM was greatly improved after GABA grafting. The initial methanol contact angle (MCA) of the PAN NFM was 132.7°, and was still 100.1° after 60 s. However, for the PAN–GABA NFM, the initial MCA was 47.8° and the complete infiltration time was only 4 s. The high wettability of the NFM was still maintained after the growth of Eu-MOF crystals. The pore size of the PAN–GABA NFM was measured by the mercury injection method, as shown in Fig. S6 (ESI†). The porosity of the NFM was up to 82.4%, and most of the pores were observed in the range of 120–431 nm with a most probable aperture of 225 nm. After growing the Eu-MOF crystals, the porosity of the NFM increased to 87.9%. High wettability and porosity would contribute to the diffusion of methanol in the MOF NFM sensor, leading to a rapid response and easy reversibility of the PAN–GABA@Eu-MOF NFM.

The excitation and emission spectra of the PAN–GABA@Eu-MOF NFM are shown in Fig. S7 (ESI†). Under excitation at 234 nm, the NFM exhibited a unique red color with four typical emission peaks at 593, 618, 650, and 699 nm, which can originate from the characteristic emission $^5D_0 \rightarrow {}^7F_J$ (J = 1–4) transitions. Fig. 3a shows the influence of GABA usage amount on the luminescence properties of the PAN–GABA@Eu-MOF NFM. The intense emission band at 618 nm ($^5D_0 \rightarrow {}^7F_2$ transition) gradually increased with the increase of GABA contents. However, the intensity of this characteristic peak barely changed when the mass ratio of PAN to GABA reached 1 : 6, suggesting that this mass ratio (1 : 6) was enough to saturate the amount of carboxyl groups on the membrane. The color change of PAN–GABA@Eu-MOF NFMs with different GABA contents under UV-light matched well with the above results, as shown in Fig. 3b. The red color of the NFM became darker as the usage amount of GABA was increased, but it was difficult to see the difference with the naked eye when the mass ratio of PAN to GABA exceeded 1 : 6, further demonstrating the saturation of carboxyl groups. The fluorescent MOF NFM can be used as a convenient fluorescent test paper for rapid and selective detection of NB. As displayed in Fig. 3c, upon dropping aromatic compounds such as NB, chlorobenzene (Cl-BZ), benzene (BZ), toluene (TO), *p*-xylene (*p*-XL), phenol (PhOH), naphthalene (NT) and bromobenzene (Br-BZ) at a concentration of 10^{-3} M on the fluorescent test paper, only NB exhibited a significant quenching effect. Moreover, competitive experiments were carried out in the presence of NB with the above mentioned aromatic compounds. Fluorescence quenching caused by the mixtures of NB with the other aromatic compounds was similar to that caused by NB alone, demonstrating that the sensing of NB by the fluorescent test paper was hardly affected by these commonly co-existent aromatic compounds. To measure the detection range of NB, different concentrations of NB solution were dropped onto the test paper. From Fig. 3d, it was clear that the fluorescence intensity gradually decreased with the increase of NB concentration. The quenching efficiency could reach 96.05% when the concentration of NB was 1×10^{-3} M, while the detectable fluorescence response of the test paper was still observed (9.15%) when the NB concentration was 1×10^{-9} M. The quenching efficiency can be quantitatively described by the Stern–Volmer (S–V) equation: $I_0/I = 1 + K_{sv}[Q]$,[23] where I_0 and I are the fluorescence intensities of the test paper and test paper with NB, respectively, $[Q]$ is the concentration of NB, and K_{sv} is the quenching constant. As displayed in Fig. S8 (ESI†), the curve presented good linearity at low concentrations (10^{-9}–10^{-6} M), whereas it gradually deviated from linearity and bent upwards at higher concentrations. This phenomenon may be due to the presence of simultaneous static and dynamic quenching.[24] The mechanism of luminescence quenching may be attributed to the energy competition between the Eu-MOF crystals and NB.[25] The luminescence of the Eu-MOF crystals resulted from the antenna effect that BTC^{3-} absorbed energy and transferred the energy to Eu^{3+}. Once NB was present, the energy absorbed by BTC^{3-} was filtered by NB. Therefore, the possibility of energy transfer from BTC^{3-} to Eu^{3+} would be reduced, consequently resulting in luminescence quenching. The UV-vis absorption spectrum of NB in Fig. S9 (ESI†) implied that the ultraviolet absorption band of NB partially overlapped with the excitation wavelength of the Eu-MOF crystals, further proving this mechanism.

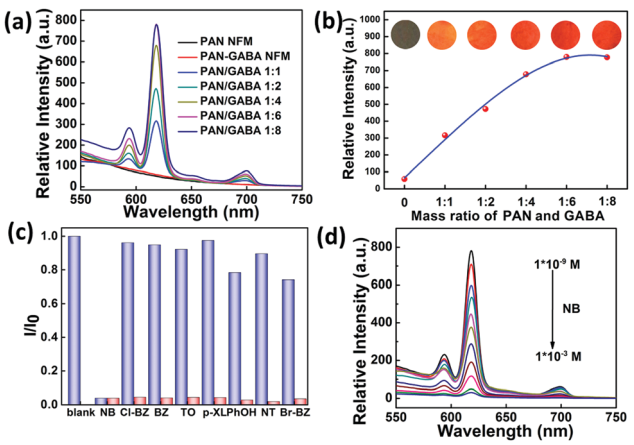

Fig. 3 Luminescence spectra (a) and relative intensities (b) of PAN–GABA@Eu-MOF NFMs with different GABA usage amounts. The insets show the corresponding photographs of the NFMs under a 265 nm UV lamp. (c) Fluorescence responses of the fluorescent test paper to various aromatic compounds (blue bars) and to mixtures of different aromatic compounds with NB (red bars). (d) Fluorescence spectra of the fluorescent test paper with different concentrations of NB.

It is very important to regenerate sensors because this can reduce the cost of the sensing process and make them more suitable for practical applications.[26] In view of this, the reversibility of the fluorescent test paper was carefully examined. As shown in Video S1 (ESI†) and Fig. 4a, an immediate fluorescence quenching was observed upon dropping NB on the fluorescent test paper, while the original red color of the test paper recovered in a very short time after dropping methanol

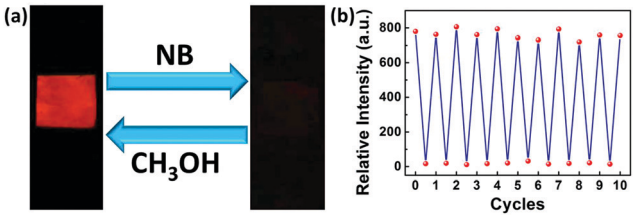

Fig. 4 (a) Reversibility test of the fluorescent test paper with NB and methanol. (b) Performance of the fluorescent test paper for the "off–on" fluorescence switching within 10 cycles.

on the test paper. Compared with powdered sensing materials, the NFM sensors needed no separation process such as centrifugation before and after recovering; hence, the "off–on" fluorescence switching process can be conducted more conveniently and rapidly. As shown in Fig. 4b, the quenching efficiency of the fluorescent test paper towards NB remained relatively stable within 10 cycles, and was approximately the same as the initial efficiency. The enhanced reversibility was primarily attributed to the stable structure of the PAN–GABA@Eu-MOF NFM. Sufficient carboxyl groups grafted onto the surface of the PAN–GABA NFM can anchor Eu-MOF particles tightly, so the morphology and structure of the fluorescent test paper remained almost unchanged after a ten-cycle experiment (Fig. S10 and S11, ESI†). Moreover, the amount of Eu^{3+} species in methanol used for recovering the test paper was determined by ICP-OES after the ten-cycle experiment. No Eu^{3+} leaching was detected in methanol, further supporting that the Eu-MOF particles was grafted strongly onto the NFM. The stability of the test paper was compared with that of the Eu-MOF/PAN NFM prepared by growing Eu-MOF crystals directly on the electrospun PAN NFM. During the regeneration process, Eu-MOF particles were obviously falling off the Eu-MOF/PAN NFM (Fig. S12b, ESI†). Due to the lack of coordination groups on the surface of the PAN NFM, Eu-MOF particles were only attached to the PAN NFM rather than growing on the surfaces of the nanofibers. Hence, the MOF particles were unstable and easily fell off the NFM (Fig. S13a, ESI†), and the fluorescence intensity of the Eu-MOF/PAN NFM gradually decreased as the number of regeneration was increased (Fig. S13b, ESI†).

In conclusion, a highly stable fluorescent NFM was successfully fabricated by *in situ* growing Eu-MOF crystals on electrospun PAN nanofibers modified with GABA. Because a great number of carboxyl groups were introduced into the nanofibrous matrix for anchoring Eu-MOF particles, the as-prepared PAN–GABA@Eu-MOF NFM was stable in the fluorescence experiments and thus could be reused multiple times with constant quenching efficiency. The NFM has been used as a convenient fluorescent test paper for rapid and cyclic detection of NB. Benefiting from the merits of the electrospun NFM, the fluorescent test paper needed no separation process before and after recovery; hence, the "off–on" fluorescence switching process can be conducted more conveniently and rapidly compared with powdered sensing materials. This work may provide new insight into the development of rapid, stable and reusable test papers based on electrospun nanofibers and MOF crystals for effective sensing detection.

This work was supported by the National Natural Science Foundation of China (Grant No. 21671090 and 21701076).

Conflicts of interest

There are no conflicts to declare.

Notes and references

1 K. Hakansson, R. V. Coorey, R. A. Zubarev, V. L. Talrose and P. Hakansson, *J. Mass Spectrom.*, 2000, **35**, 337–346.
2 J. M. Sylvia, J. A. Janni, J. D. Klein and K. M. Spencer, *Anal. Chem.*, 2000, **72**, 5834–5840.
3 M. Krausa and K. Schorb, *J. Electroanal. Chem.*, 1999, **461**, 10–13.
4 S. J. Toal and W. C. Trogler, *J. Mater. Chem.*, 2006, **16**, 2871–2883.
5 X. Sun, Y. Wang and Y. Lei, *Chem. Soc. Rev.*, 2015, **44**, 8019–8061.
6 Y. Salinas, R. Martínez-Máñez, M. D. Marcos, F. Sancenón, A. M. Costero, M. Parra and S. Gil, *Chem. Soc. Rev.*, 2012, **41**, 1261–1296.
7 Z. Hu, B. J. Deibert and J. Li, *Chem. Soc. Rev.*, 2014, **43**, 5815–5840.
8 (*a*) N. Wei, R. X. Zuo, Y. Y. Zhang, Z. B. Han and X. J. Gu, *Chem. Commun.*, 2017, **53**, 3224–3227; (*b*) Y. Zhang, Y. X. Wang, L. Liu, N. Wei, M. L. Gao, D. Zhao and Z. B. Han, *Inorg. Chem.*, 2018, **57**, 2193–2198; (*c*) L. Liu, S. M. Wang, Z. B. Han, M. L. Ding, D. Q. Yuan and H. L. Jiang, *Inorg. Chem.*, 2016, **55**, 3558–3565.
9 (*a*) Y.-L. Hou, H. Xu, R.-R. Cheng and B. Zhao, *Chem. Commun.*, 2015, **51**, 6769–6772; (*b*) C.-S. Liu, Z.-H. Zhang, M. Chen, H. Zhao, F.-H. Duan, D.-M. Chen, M.-H. Wang, S. Zhang and M. Du, *Chem. Commun.*, 2017, **53**, 3941–3944.
10 (*a*) Y. Cui, B. Chen and G. Qian, *Coord. Chem. Rev.*, 2014, **273-274**, 76–86; (*b*) S. V. Eliseeva and J.-C. G. Bünzli, *Chem. Soc. Rev.*, 2010, **39**, 189–227.
11 (*a*) X.-M. Lin, J.-L. Niu, P.-X. Wen, Y. Pang, L. Hu and Y.-P. Cai, *Cryst. Growth Des.*, 2016, **16**, 4705–4710; (*b*) R.-C. Gao, F.-S. Guo, N.-N. Bai, Y.-L. Wu, F. Yang, J.-Y. Liang, Z.-J. Li and Y.-Y. Wang, *Inorg. Chem.*, 2016, **55**, 11323–11330.
12 (*a*) J. Zhao, X. Wang, L. Liu, J. Yu and B. Ding, *ACS Appl. Mater. Interfaces*, 2018, **10**, 30887–30894; (*b*) J. Ge, D. Zong, Q. Jin, J. Yu and B. Ding, *Adv. Funct. Mater.*, 2018, **28**, 1705051.
13 C. Kim, J.-Y. Hwang, K.-S. Ku, S. Angupillai and Y.-A. Son, *Sens. Actuators, B*, 2016, **228**, 259–269.
14 Y. Zhang, Y. Zhang, X. Wang, J. Yu and B. Ding, *ACS Appl. Mater. Interfaces*, 2018, **10**, 34802–34810.
15 Y. Zhang, S. Yuan, X. Feng, H. Li, J. Zhou and B. Wang, *J. Am. Chem. Soc.*, 2016, **138**, 5785–5788.
16 A. X. Lu, M. McEntee, M. A. Browe, M. G. Hall, J. B. DeCoste and G. W. Peterson, *ACS Appl. Mater. Interfaces*, 2017, **9**, 13632–13636.
17 C. Wang, T. Zheng, R. Luo, C. Liu, M. Zhang, J. Li, X. Sun, J. Shen, W. Han and L. Wang, *ACS Appl. Mater. Interfaces*, 2018, **10**, 24164–24171.
18 Y. Xu, Y. Wen, W. Zhu, Y.-N. Wu, C. Lin and G. Li, *Mater. Lett.*, 2012, **87**, 20–23.
19 R. Ostermann, J. Cravillon, C. Weidmann, M. Wiebcke and B. M. Smarsly, *Chem. Commun.*, 2011, **47**, 442–444.
20 A. Centrone, Y. Yang, S. Speakman, L. Bromberg, G. C. Rutledge and T. A. Hatton, *J. Am. Chem. Soc.*, 2010, **132**, 15687–15691.
21 P. K. Neghlani, M. Rafizadeh and F. A. Taromi, *J. Hazard. Mater.*, 2011, **186**, 182–189.
22 X. Guo, G. Zhu, Z. Li, F. Sun, Z. Yang and S. Qiu, *Chem. Commun.*, 2006, 3172–3174.
23 S. W. Thomas, G. D. Joly and T. M. Swager, *Chem. Rev.*, 2007, **107**, 1339–1386.
24 A. A. O. El-Ballouli, E. Alarousu, M. Bernardi, S. M. Aly, A. P. Lagrow, O. M. Bakr and O. F. Mohammed, *J. Am. Chem. Soc.*, 2014, **136**, 6952–6959.
25 H. Xu, F. Liu, Y. J. Cui, B. L. Chen and G. D. Qian, *Chem. Commun.*, 2011, **47**, 3153–3155.
26 Y. Li, Y. Wen, L. Wang, J. He, S. S. Al-Deyab, M. El-Newehy, J. Yu and B. Ding, *J. Mater. Chem. A*, 2015, **3**, 18180–18189.

